Inorganic Chemistry

Article

pubs.acs.org/IC

Series of Structural and Functional Models for the ES (Enzyme–Substrate) Complex of the Co(II)-Containing Quercetin 2,3-Dioxygenase

Ying-Ji Sun,* Qian-Qian Huang, and Jian-Jun Zhang

School of Chemistry, Dalian University of Technology, 2 Linggong Road, Dalian 116024, China

Supporting Information

ABSTRACT: A series of mononuclear Co^{II}–flavonolate complexes $[Co^{II}L^{R}(fla)]$ ($\mathbf{L^{R}H}$ = 2-{[bis(pyridin-2-ylmethyl)-amino]methyl}-*p*/*m*-R-benzoic acid; R = *p*-OMe (**1**), *p*-Me (**2**), *m*-Br (**4**), and *m*-NO_2 (**5**); fla = flavonolate) were designed and synthesized as structural and functional models for the ES (enzyme–substrate) complexes to mimic the active site of the Co(II)-containing quercetin 2,3-dioxygenase (Co–2,3-QD). The metal center Co(II) ion in each complex shows a similar distorted octahedral geometry. The model complexes display high enzyme-type dioxygenation reactivity (oxidative *O*-heterocyclic ring opening of the coordinated substrate flavonolate) at low temperature, presumably due to the attached carboxylate group in the ligands. The reactivity exhibits a substituent group dependent order of –OMe (**1**) > –Me (**2**) > –H (**3**)[14b] > –Br (**4**) > –NO_2 (**5**), and the Hammett plot is linear (ρ = −0.78). This can be explained as the electronic nature of the substituent group in the ligands may influence the conformation and redox potential of the bound flavonolate and finally bring different reactivity. The structures, properties, and reactivity of the model complexes show some dependence on the substituent group in the supporting model ligands, and there is some relationship among them. This study is the first example of a series of structural and functional ES models of Co–2,3-QD, with focus on the effects of the electronic nature of substituted groups and the carboxylate group of the ligands to the dioxygenation reactivity, that will provide important insights into the structure–property–reactivity relationship and the catalytic role of Co–2,3-QD.

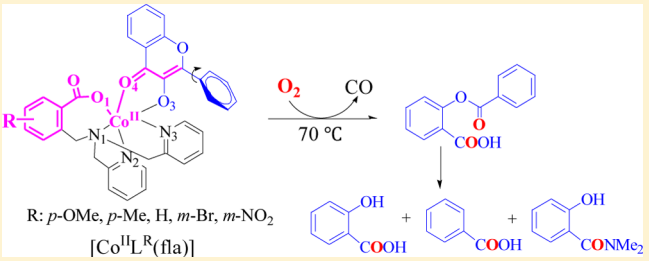

INTRODUCTION

Co ion plays an important role in many biological processes. It is mainly included in coenzyme B_{12};[1] however, there are various kinds of Co(II)-substituted enzymes. Most of them are nonredox zinc(II) enzymes,[2] while Co(II) substitution is also found in some oxidoreductase, such as amine oxidase (Cu),[3a] catechol dioxygenase (Fe),[3b] acireductone dioxygenase (ARD) (Fe and Ni),[3c] and quercetin 2,3-dioxygenase (2,3-QD) (Cu and Fe).[4] The iron-containing dioxygenase has been extensively studied; however, the noniron metal, especially the Co(II)-containing dioxygenases, received much less attention until recently. The metal diversity among the various kinds of dioxygenases for catalysis and the variability in metal cofactor selectivity in the same dioxygenase are a very interesting and poorly understood field and will be a topic of future study.

Quercetin 2,3-dioxygenase (2,3-QD) catalyzes the oxygenative ring-opening reaction of the *O*-heterocycle of quercetin (3′,4′,5,7-tetrahydroxyflavonol, QUE) to the corresponding depside (phenolic carboxylic acid esters) and carbon monoxide by activation of dioxygen (Scheme 1) .[5]

The mononuclear M(II) (M = Cu, Fe) active sites of 2,3-QD from *Aspergillus japonicus*[6] and *Bacillus subtilis*[4a,7] have similar structure. Each of them shows two distinct coordination environments. One is distorted trigonal-bipyramidal geometry, and the M(II) ion is coordinated by three histidine imidazoles, one water molecule, and one carboxylate group of Glu. Another is a distorted tetrahedral or square pyramidal geometry, depending on whether there is not or is an additionally weak interaction of the carboxylate group of Glu.

Under anaerobic conditions, the deprotonated substrate was coordinated to the Cu(II) center via displacement of the water molecule to form an ES (enzyme–substrate) complex.[8] Site-directed mutagenesis experiments show that the enzyme activity was lost by mutation of Glu73,[6] indicating that the carboxylate group of Glu73 plays an important role in the catalytic reaction. It may act as an active site base to deprotonate the substrate, help to stabilize the bound substrate through a hydrogen bond, modulate the redox potential of the metal ion, and lower the energy barriers.[6,9]

Scheme 1

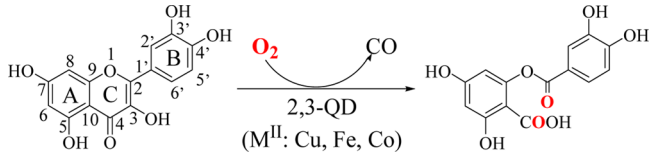

Received: October 26, 2013
Published: March 6, 2014

   dx.doi.org/10.1021/ic402695c | *Inorg. Chem.* 2014, 53, 2932–2942

Metal-replacement experiments of the native Fe(II)-containing 2,3-QD from *B. subtilis* demonstrate that the Co(II)- and Mn(II)-substituted enzymes show 24- and 35-times increased catalytic activity relative to the native enzyme, respectively.[4b] A recent study of 2,3-QD from *Streptomyces* sp. FLA (monocupin) has shown that the Ni(II)- and Co(II)-containing enzymes exhibit the highest and next highest level of reactivity.[4c] These results clearly indicate that the catalytic activity of the enzymes are remarkably affected by the metal ions, and the 2,3-QD enzymes have surprising variability in metal cofactor selectivity and structural flexibility for the metal cofactor.[4,7]

Generally, the amino acid residues of/around the active site of the enzyme and their substituent groups could influence the properties and catalytic activity of the enzyme by affecting the coordination environment of the metal cofactor and the conformation of the enzyme. However, detailed roles of the electronic nature, carboxylate group, and metal ion on the catalytic mechanism are not clear.

To date, most of the reported 2,3-QD model complexes are Cu(II) based,[10,16,17] and little attention has been paid to other transition-metal ions,[11−15] especially the Co(II) complexes.[12−14] Nishinaga's group reported $[Co^{II}(salen)]$/$[Co^{III}(salen)(OH)]$ ($salenH_2$ = 1,6-bis-(2-hydroxyphenyl)-2,5-diaza-hexa-1,5-diene) could be used as catalyst in the dioxygenation of the substrate flavonol derivatives at room temperature.[12a,b] The electronic substituent effects of the substrate flavonol and solvent effects on the catalytic reactivity were also discussed. They also reported a series of $[Co^{III}(4'/7R\text{-fla})(5'/5R\text{-salen})]$ (fla = flavonolate)[12c,d] 2,3-QD model complexes; however, no detailed kinetic study was reported. Thus far, $[Co^{III}(fla)(salen)]$,[12c] $[(6\text{-}Ph_2TPA)Co^{II}(fla)]ClO_4$ (6-Ph_2TPA = *N*,*N*-bis((6-phenyl-2-pyridyl)methyl)-*N*-((2-pyridyl)methyl)amine),[13a] and $[Co^{II}L^{H}(fla)]$ (**3**) ($L^{H}H$ = 2-{[bis(pyridin-2-ylmethyl)amino]methyl}benzoic acid)[14b] are the only three examples of the structurally characterized Co−flavonolate complexes. However, in $[Co^{III}(fla)(salen)]$ the oxidation state of Co ion is different from that of Co-2,3-QD. Kinetic study of $[(6\text{-}Ph_2TPA)Co^{II}(fla)]ClO_4$ indicates it displays "dioxygenase-type reactivity" upon being irradiated by UV light.[13b] Our previously reported $[Co^{II}L^{H}(fla)]$ (**3**)[14b] is the only structurally characterized ES-model complex of Co-2,3-QD with enzyme-type dioxygenation reactivity. The observed higher dioxygenation reactivity of $[Co^{II}L^{H}(fla)]$ (**3**)[14b] sparked our interest to further study the role of the higher potential Co(II) center in O_2 activation and the C−C bond cleavage process.

Most of the model ligands used in the model complexes of 2,3-QD are polyamine *N*-chelating ligands;[10−13,15,16] the role of active site carboxylate group of Glu has received much less attention. Two reports[11c,16] focused on the reactivity of model complexes of 2,3-QD also reveal that dioxygenation of the bound substrate flavonolate can be promoted by addition of excess free carboxylate ligands, due to the change of coordination mode of the bound substrate flavonolate from bidentate to monodentate resulting from coordination of the exogenous carboxylate. Thus far, five types of ligands bearing a carboxylate group were used in 2,3-QD model complexes,[14,17] but the effect of the introduced carboxylate group on the reactivity was not observed except $[M^{II}L^{H}(fla)]$.[14b] Besides, several biomimetic studies about the electronic effects of the substituted groups of the substrate flavonol on the reactivity have been reported.[10,11c,15] However, no example about the electronic substituent effects of the supporting model ligands on the reactivity was reported.

To gain insights into the electronic substituent effects and the carboxylate effects of the supporting model ligand on the catalytic role of Co-2,3-QD, we herein designed and synthesized a series of Co^{II}−flavonolate complexes $[Co^{II}L^{R}(fla)]$ supported by the *p*/*m*-substituted carboxylate ligand L^{R} ($L^{R}H$ = 2-{[bis(pyridin-2-ylmethyl)amino]methyl}-*p*/*m*-R-benzoic acid (Figure 1); R = *p*-OMe (**1**), *p*-Me (**2**), *m*-Br (**4**), and *m*-NO_2 (**5**); fla = flavonolate) as structural and functional ES models of Co−2,3-QD. Details of their structures, spectroscopic features, redox properties, and reactivity toward dioxygen are discussed.

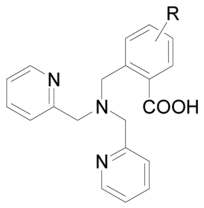

R: *p*-OMe, *p*-Me, H, *m*-Br, *m*-NO_2

$L^{R}H$

Figure 1. Structure of ligand $L^{R}H$.

EXPERIMENTAL SECTION

General and Physical Methods. All chemicals used in this study except the ligands and complexes were commercial products of the highest available purity and further purified by the standard method[18] if necessary. FT-IR spectra were recorded with a Nicolet 6700 spectrophotometer. UV−vis spectra were measured using an Agilent Technologies HP8453 diode array spectrophotometer. ESI-MS (electrospray ionization mass spectra) measurements were performed on an Agilent Technologies HP1100LC-MSD. ^{1}H NMR spectra were recorded on a Bruker 400WB. EPR spectra were obtained on a Bruker MEX-Plus spectrometer fitted with a liquid helium cooled probe. Spectra of the complexes (4 mM in 0.5 mL of DMF) were recorded at −173 °C, about 20 mW microwave powers, and about 9.40 GHz. The sample was put into a nitric acid washed quartz EPR tube and frozen in liquid nitrogen. Cyclic voltammetry data was collected using a CHI620b system. All CV data were obtained under N_2 in DMF with a complex concentration of 2 mM and $KClO_4$ (0.5 M) as the supporting electrolyte. The experimental setup consisted of a glassy carbon working electrode, an SCE reference electrode, and a platinum wire auxiliary electrode. All potentials are reported versus SCE. HPLC-MS measurements were performed on a Thermo Fisher Scientific LTQ Orbitrap XL HPLC-MS.

X-ray Crystallography. All single crystals of the complexes were mounted on a glass capillary. X-ray diffraction data were collected by a Bruker Smart APEXII CCD single-crystal diffractometer using Mo Kα radiation (λ = 0.71073 Å) to $2\theta_{max}$ of 50−55.0° at 296 K. Crystallographic calculations were performed by a combination of direct and heavy atom methods using SHELXTL 97.[19] All non-hydrogen and hydrogen atoms were refined anisotropically and isotropically.

Kinetic Measurements. *$[Co^{II}L^{R}(fla)]$ Dependence.* The reactions of the complexes $[Co^{II}L^{R}(fla)]$ with O_2 were performed in a 10 mm path length UV−vis cell that was held in a Unisoku thermostatted cell holder USP-203 (a desired temperature can be fixed within ±0.5 °C). After the solution (3 mL of DMF) of $[Co^{II}L^{R}(fla)]$ ($0.78−1.7 \times 10^{-4}$ M) was kept at a desired temperature (70 °C) under N_2 for several minutes, the N_2 was replaced with O_2. The time courses of the reactions were followed by monitoring the absorption changes at a λ_{max} due to the $\pi \rightarrow \pi^*$ transition of the coordinated flavonolate. The

dx.doi.org/10.1021/ic402695c | *Inorg. Chem.* 2014, 53, 2932−2942

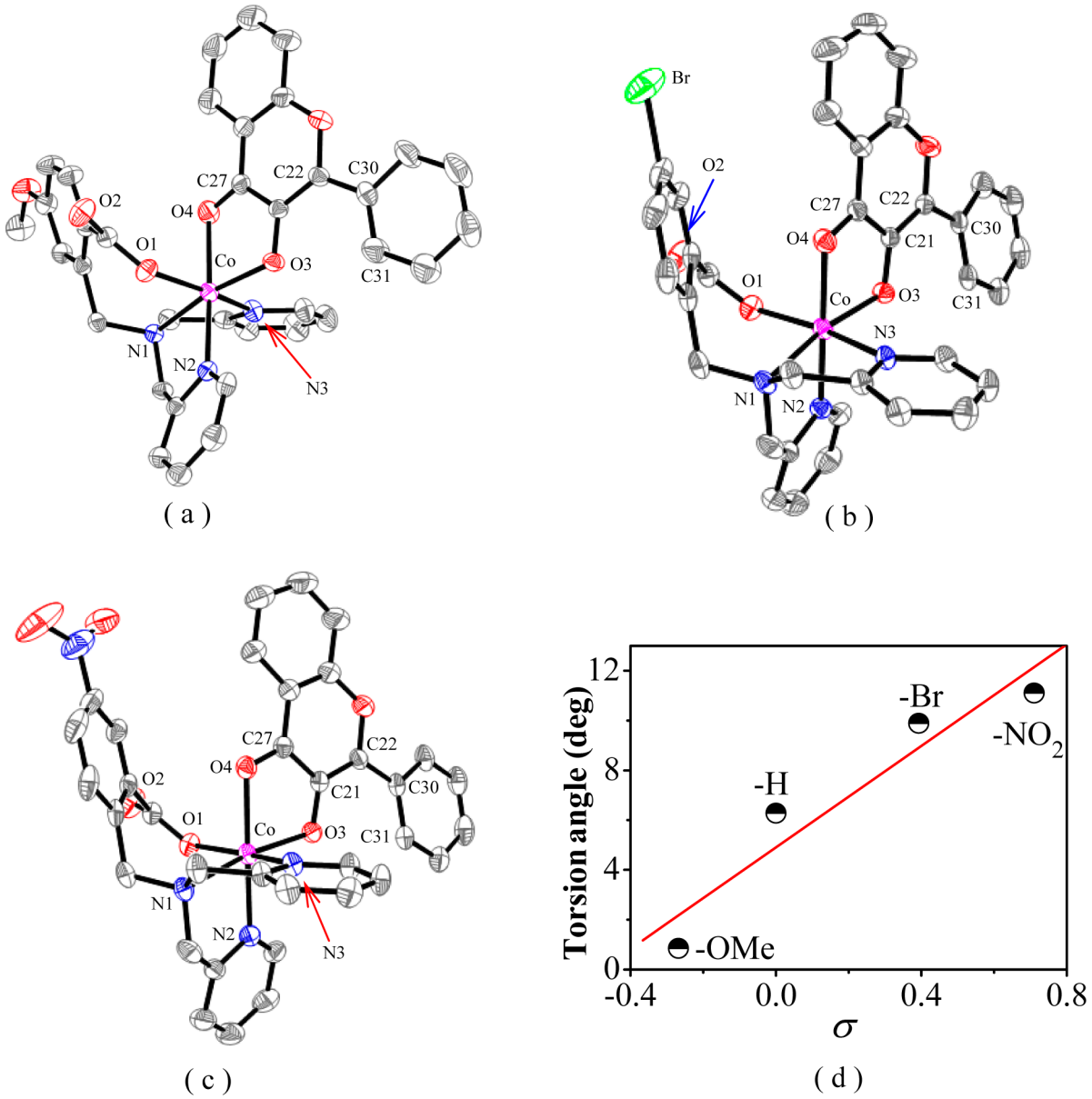

Figure 2. ORTEP representation of (a) $[Co^{II}L^{OMe}(fla)]\cdot CH_3OH$ (**1**), (b) $[Co^{II}L^{Br}(fla)]\cdot CH_3OH\cdot H_2O$ (**4**), and (c) $[Co^{II}L^{NO2}(fla)]\cdot Et_2O\cdot 0.5H_2O$ (**5**). (d) Plot of the torsion angle at C(21)− C(22)− C(30)− C(31) vs Hammett constants σ. Ellipsoids are shown at the 50% probability level. Hydrogen atoms and solvent molecules are omitted for clarity.

initial concentrations of $[Co^{II}L^{R}(fla)]$ were determined using the ε value at the λ_{max} of each complex (see Table 3).

O_2 Dependence. In a typical experiment, $[Co^{II}L^{R}(fla)]$ (1.0×10^{-4} M in 60 mL of DMF) was kept under N_2 for several minutes in a thermostatted reaction vessel connecting to a manometer to regulate constant dioxygen pressure. The solution was then heated to the desired temperature (60−75 ± 0.5 °C), and the N_2 was replaced with O_2. The reaction mixture was taken by syringe periodically (ca. every 2 min), and the time courses of the reactions were followed by monitoring the absorption changes at a λ_{max} due to the $\pi \rightarrow \pi^*$ transition of the coordinated flavonolate. O_2 concentrations were calculated from literature data[20] taking into account the partial pressure of DMF[21] and assuming the validity of Dalton's law.

Determination of the Activation Parameters. The activation parameters for degradation of $[Co^{II}L^{R}(fla)]$ were obtained from an Eyring plot (Table 4, Supporting Information, Table S3 and Figure S5) with $[Co^{II}L^{R}(fla)]$ (1.0×10^{-4} M) at the temperature range of 55−85 °C. The experimental procedures were similar to the kinetic study described above.

Reaction Product Analysis. $[Co^{II}L^{R}(fla)]$ (2.0×10^{-3} M in 2 mL of DMF) was stirred at 70 °C for 8 h under O_2. After the reaction, the mixture was concentrated by evaporation and the remaining residue was dissolved in 1.9 mL of MeOH. *o*-Methylbenzoic acid (10 mM in 100 μL of MeOH solution, total 0.5 mM in 2.0 mL of solution) was added to the above solution as an internal standard, and the reaction products were analyzed with a Thermo Fisher Scientific LTQ Orbitrap XL HPLC-MS with an online UV−vis detector (λ: 210 nm). A Hypersil GOLD C18 column (Thermo Fisher Scientific 150 mm × 2.1 mm, 5 μm) was used for HPLC analysis at room temperature with a mobile phase (MeOH and 5 mM NH_4OAc) with some gradient at a constant flow rate of 0.5 mL min^{-1}. The yields of the reaction products were calculated using the standard calibration curve.

Synthesis of the Model Ligands and Complexes. The synthesis and characterization details of the model ligands $\mathbf{L^RH}$ (R = *p*-OMe, *p*-Me, *m*-Br, and *m*-NO_2) are shown in the Supporting Information.

General Procedure for Synthesis of $[Co^{II}L^{R}(fla)]$. Under a nitrogen atmosphere, a dry CH_3OH (1.0 mL) solution of $\mathbf{L^RH}$ (0.05 mmol)

dx.doi.org/10.1021/ic402695c | Inorg. Chem. 2014, 53, 2932−2942

Table 1. Summary of X-ray Data Collection and Refinement

	$[Co^{II}L^{OMe}(fla)]\cdot CH_3OH$ (**1**)	$[Co^{II}L^{Br}(fla)]\cdot CH_3OH\cdot H_2O$ (**4**)	$[Co^{II}L^{NO2}(fla)]\cdot Et_2O\cdot 0\cdot 5H_2O$ (**5**)
empirical formula	$C_{37}H_{33}CoN_3O_7$	$C_{36}H_{32}BrCoN_3O_7$	$C_{39}H_{37}CoN_4O_{8.50}$
M_r	690.59	757.49	756.66
cryst syst	orthorhombic	monoclinic	monoclinic
space group	*Pbca*	*P*2(1)/*c*	*P*2(1)/*c*
a/Å	9.6655(10)	8.9469(6)	8.8402(4)
b/Å	22.650(2)	17.8871(9)	18.0551(8)
c/Å	30.634(3)	23.1484(14)	23.3936(14)
α/deg	90	90	90
β/deg	90	99.073(4)	97.638(3)
γ/deg	90	90	90
V/Å^3	6706.5(12)	3658.2(4)	3700.7(3)
Z	8	4	4
d_{calcd}/g cm^{-3}	1.368	1.375	1.358
T/K	296(2)	296(2)	296(2)
cryst habit	prism	prism	prism
color	wine red	wine red	wine red
cryst size (mm^3)	0.20 × 0.15 × 0.10	0.30 × 0.25 × 0.20	0.25 × 0.18 × 0.12
μ/mm^{-1}	0.566	1.611	0.523
$2\theta_{max}$/deg	55.00	50.00	52.00
completeness to θ (%)	99.7	99.7	99.7
no. of reflns collected	43 075	13 154	14 550
no. of independent reflns	7682	6429	7247
R_{int}	0.0606	0.0304	0.0392
variable params	433	432	454
$R1^a/wR2^b$	0.0568/0.1714	0.0668/0.2297	0.0540/0.1527
goodness-of-fit on F^2	1.043	1.026	1.006
$\Delta\rho_{max/min}$/e Å^{-3}	0.973/−0.433	1.901/−0.911	0.432/−0.436

$^a R1 = \sum(||F_o| - |F_c||)/\sum|F_o|$. $^b wR2 = [\sum w (F_o^2 - F_c^2)^2/\sum w(F_o^2)^2]^{1/2}$, where $w = 1/[\sigma^2(F_o^2) + (aP)^2 + bP]$.

Table 2. Selected Bond Distances (Angstroms) and Bond Angles (degrees) for the Complexes

	$[Co^{II}L^{OMe}(fla)]\cdot CH_3OH$ (**1**)	$[Co^{II}L^{Br}(fla)]\cdot CH_3OH\cdot H_2O$ (**4**)	$[Co^{II}L^{NO2}(fla)]\cdot Et_2O\cdot 0\cdot 5H_2O$ (**5**)
Co(1)−O(1)	2.035(2)	2.050(3)	2.058(2)
Co(1)−O(3)	1.997(2)	2.012(3)	2.007(2)
Co(1)−O(4)	2.157(2)	2.138(3)	2.150(2)
Co(1)−N(1)	2.194(2)	2.212(4)	2.219(3)
Co(1)−N(2)	2.131(3)	2.104(4)	2.111(3)
Co(1)−N(3)	2.163(3)	2.151(4)	2.132(3)
O(3)−C(21)	1.310(4)	1.308(5)	1.301(4)
O(4)−C(27)	1.250(4)	1.242(5)	1.249(4)
C(21)−C(22)	1.378(4)	1.392(6)	1.388(4)
O(1)−Co(1)−O(3)	99.92(9)	100.40(13)	101.46(9)
O(1)−Co(1)−O(4)	87.79(10)	90.25(13)	88.92(9)
O(1)−Co(1)−N(1)	90.59(9)	89.53(13)	88.78(9)
O(1)−Co(1)−N(2)	86.30(9)	86.86(14)	87.31(10)
O(1)−Co(1)−N(3)	163.19(10)	164.87(14)	163.56(9)
O(3)−Co(1)−N(1)	168.69(10)	169.33(14)	168.86(9)
O(3)−Co(1)−N(2)	96.94(9)	96.75(14)	96.10(10)
O(3)−Co(1)−N(3)	94.73(10)	94.11(13)	94.11(9)
O(3)−Co(1)−O(4)	80.15(9)	79.74(12)	79.68(9)
O(4)−Co(1)−N(1)	104.59(9)	104.29(14)	105.16(9)
O(4)−Co(1)−N(2)	172.87(10)	175.00(14)	173.68(10)
O(4)−Co(1)−N(3)	86.63(10)	88.16(14)	88.69(9)
N(1)−Co(1)−N(2)	79.47(9)	79.79(15)	79.85(10)
N(1)−Co(1)−N(3)	75.53(10)	76.31(13)	76.17(9)
N(2)−Co(1)−N(3)	100.15(10)	95.69(15)	96.35(10)
torsion angle at C(21)−C(22)−C(30)−C(31)	−0.914(12)	−9.876(7)	−11.030(7)

was added dropwise to a dry CH_3OH solution (1.0 mL) of $Co(OAc)_2\cdot 4H_2O$ (12.8 mg, 0.05 mmol) at room temperature. After stirring for 30 min, a CH_3OH/CH_2Cl_2 (1:1) solution containing flavonol (11.9 mg, 0.05 mmol) and $Me_4NOH\cdot 5H_2O$ (9.05 mg, 0.05 mmol) was added

dx.doi.org/10.1021/ic402695c | Inorg. Chem. 2014, 53, 2932−2942

dropwise to the above solution; then the mixture was stirred for 1 day under N_2. $[Co^{II}L^{R}(fla)]$ was isolated as a reddish-yellow powder by filtration. Wine red single crystals of $[Co^{II}L^{OMe}(fla)]$ (**1**), $[Co^{II}L^{Br}(^{-}a)]$ (**4**), and $[Co^{II}L^{NO2}(fla)]$ (**5**) suitable for X-ray crystallographic analysis were obtained by slow diffusion of ether into the dichloromethane solution of the complexes at −20 °C.

$[Co^{II}L^{OMe}(fla)]\cdot CH_3OH$ (1). Yield: 23.7 mg, 69%. ESI-MS: *m*/*z* (pos.) = 659.1 ($[Co^{II}L^{OMe}(fla)]H^+$) (main peak), 681.3 ($[Co^{II}L^{OMe}(^{-}a)]$-Na^+). Anal. Calcd for $C_{37}H_{33}CoN_3O_7$ (690.59): C, 64.35; H, 4.82; N, 6.08. Found: C, 64.46; H, 4.93; N, 6.19. FT-IR (solid sample, KBr, cm^{-1}): 3485 (m), 1593 (s), 1558 (s), 1485 (m), 1412 (m), 1388 (w), 1217 (s), 1101 (m), 760 (m). FT-IR (solution sample, in ethanol, cm^{-1}): 3343 (m), 1614 (s), 1549 (s), 1487 (m), 1416 (m), 1381 (w), 1217 (s), 754 (m).

$[Co^{II}L^{Me}(fla)]\cdot CH_3OH$ (2). Yield: 19.3 mg, 57%. ESI-MS: *m*/*z* (pos.) = 643.3 ($[Co^{II}L^{Me}(fla)]H^+$) (main peak), 665.3 ($[Co^{II}L^{Me}(fla)]Na^+$). Anal. Calcd for $C_{37}H_{33}CoN_3O_6$ (674.61): C, 65.87; H, 4.93; N, 6.23. Found: C, 65.73; H, 5.02; N, 6.36. FT-IR (solid sample, KBr, cm^{-1}): 3480 (m), 1610 (s), 1550 (s), 1490 (m), 1420 (s), 1360 (w), 1220 (s), 907 (m), 755 (s). FT-IR (solution sample, in ethanol, cm^{-1}): 3346 (m), 1590 (s), 1557 (s), 1486 (m), 1409 (s), 1353 (w), 1214 (s), 906 (w), 757 (s).

$[Co^{II}L^{Br}(fla)]\cdot CH_3OH\cdot H_2O$ (4). Yield: 29.3 mg, 77%. ESI-MS: *m*/*z* (pos.) = 707.1 ($[Co^{II}L^{Br}(fla)]H^+$), 729.1 ($[Co^{II}L^{Br}(fla)]Na^+$) (main peak). Anal. Calcd for $C_{36}H_{32}BrCoN_3O_7$ (757.49): C, 57.08; H, 4.26; N, 5.55. Found: C, 57.21; H, 4.36; N, 5.69. FT-IR (solid sample, KBr, cm^{-1}): 3440 (m), 1610 (s), 1560 (s), 1480 (m), 1410 (s), 1350 (m), 1220 (s), 1150 (w), 906 (w), 754 (s). FT-IR (solution sample, in ethanol, cm^{-1}): 3357 (m), 1603 (s), 1553 (s), 1482 (s), 1410 (s), 1352 (m), 1215 (s), 1148 (w), 752 (s).

$[Co^{II}L^{NO2}(fla)]\cdot Et_2O\cdot 0.5H_2O$ (5). Yield: 26.2 mg, 70%. ESI-MS: *m*/*z* (pos.) = 674.0 ($[Co^{II}L^{NO2}(fla)]H^+$) (main peak), 696.0 ($[Co^{II}L^{NO2}(fla)]Na^+$). Anal. Calcd for $C_{39}H_{37}CoN_4O_{8.50}$ (756.66): C, 61.91; H, 4.93; N, 7.40. Found: C, 62.04; H, 5.01; N, 7.54. FT-IR (solid sample, KBr, cm^{-1}): 3480 (m), 1614 (w), 1551 (s), 1487 (m), 1418 (s), 1321 (m), 1217 (s), 908 (w), 754 (s), 669 (s). FT-IR (solution sample, in ethanol, cm^{-1}): 3334 (m), 1604 (w), 1558 (s), 1485 (m), 1414 (s), 1346 (s), 1215 (w), 1155 (w), 759 (s).

RESULTS AND DISCUSSION

Synthesis and Structural Characterization. Four new model ligands bearing carboxylate group $\mathbf{L^RH}$ (R = *p*-OMe, *p*-Me, *m*-Br, and *m*-NO_2) (Figure 1) were designed and synthesized, and their corresponding cobalt(II) complexes $[Co^{II}L^{R}(fla)]$ (R = *p*-OMe (**1**), *p*-Me (**2**), *m*-Br (**4**), and *m*-NO_2 (**5**)) were synthesized by mixing 1 equiv of $Co(OAc)_2\cdot 4H_2O$, ligand L^RH, $Me_4NOH\cdot 5H_2O$, and flavonol in MeOH/CH_2Cl_2 under N_2. All complexes are relatively stable under air in the solid state but react with O_2 in solution (see below).

The single-crystal X-ray structures of the complexes $[Co^{II}L^{OMe}(fla)]\cdot CH_3OH$ (**1**), $[Co^{II}L^{Br}(fla)]\cdot CH_3OH\cdot H_2O$ (**4**), and $[Co^{II}L^{NO2}(fla)]\cdot Et_2O\cdot 0.5H_2O$ (**5**) are shown in Figure 2a, 2b, and 2c, respectively. Crystallographic data of the complexes are summarized in Table 1. Selected bond distances and angles are listed in Table 2. The structures of the complexes are similar to each other and also similar to that of the nonsubstituted analogue $[Co^{II}L^{H}(fla)]\cdot CH_3OH$ (**3**),[14b] all bearing a distorted octahedral metal center, which is coordinated by two oxygen atoms from flavonolate (O(3), 3-hydroxylate; O(4), 4-carbonyl), one carboxylate oxygen O(1), and three nitrogen atoms from L^R. Interestingly, their crystal systems and space groups vary with the substituent group of the ligands. $[Co^{II}L^{OMe}(fla)]\cdot CH_3OH$ (**1**) with an electron-donating group crystallizes in the orthorhombic system and *Pbca* space group, which is similar to that of the nonsubstituted analogue $[Co^{II}L^{H}(fla)]\cdot CH_3OH$ (**3**).[14b] In contrast, $[Co^{II}L^{Br}(fla)]\cdot CH_3OH\cdot H_2O$ (**4**) and $[Co^{II}L^{NO2}(fla)]\cdot Et_2O\cdot 0.5H_2O$ (**5**) with electron-withdrawing groups crystallize in the monoclinic system and *P*2(1)/*c* space group.

The Co−O(1) (benzoate of L^R) bond distance is 2.035(2) Å for **1**, 2.050(3) Å for **4**, and 2.058(2) Å for **5**, which is close to that of $[Co^{II}L^{H}(fla)]\cdot CH_3OH$ (**3**) (2.0165(14) Å).[14b] The bond lengths of Co−O(3) and Co−O(4) are 1.997(2) and 2.157(2) Å for **1**, 2.012(3) and 2.138(3) Å for **4**, and 2.007(2) and 2.150(2) Å for **5**, respectively, which are similar to those of $[Co^{II}L^{H}(fla)]\cdot CH_3OH$ (**3**) (1.9993(14) and 2.1797(14) Å)[14b] and $[Co^{II}(6\text{-}Ph_2TPA)(fla)]ClO_4$ (1.956(2) and 2.172(2) Å).[13a] The difference [Δd(Co−O)] between Co−O(3) and Co−O(4) is 0.16 Å for **1**, 0.13 Å for **4**, and 0.14 Å for **5**, which are also close to those of $[Co^{II}L^{H}(fla)]\cdot CH_3OH$ (**3**) (0.18 Å)[14b] and $[Co^{II}(6\text{-}Ph_2TPA)(fla)]ClO_4$ (0.22 Å).[13a] The average Co−N bond distance is 2.16 Å for both **1** and **4** and 2.15 Å for **5**, which are similar to those of $[Co^{II}L^{H}(fla)]\cdot CH_3OH$ (**3**) (2.16 Å)[14b] and $[Co^{II}(6\text{-}Ph_2TPA)(fla)]ClO_4$ (2.22 Å).[13a] Besides, bond valence calculation[22] (2.04 for **1**, 2.05 for both **4** and **5**) also proves the metal center is the +2 state, which is in good agreement with ESI-MS, EPR, and magnetic moment results described below.

It should be noted that there are some structural and conformational changes in the bound substrate flavonolate. The distances of C(21)−O(3) (3-hydroxylate) (1.310(4) Å for **1**, 1.308(5) Å for **4**, and 1.301(4) Å for **5**) are slightly contracted relative to that of free flaH (1.357(3) Å).[23] In contrast, the distances of C(27)=O(4) (4-carbonyl) (1.250(4) Å for **1**, 1.242(5) Å for **4**, and 1.249(4) Å for **5**) and C(21)=C(22) (1.378(4) Å for **1**, 1.392(6) Å for **4**, and 1.388(4) Å for **5**) are slightly elongated relative to that of free flavonol (1.232(3) and 1.363(4) Å).[23] However, all are close to the corresponding distances in $[Co^{II}L^{H}(fla)]\cdot CH_3OH$ (**3**) (1.313(2), 1.259(2), and 1.376(2) Å).[14b] It should be noted that the elongated C=C bond may be helpful for its cleavage during the dioxygenation reaction described below (Scheme 3). Interestingly, the B ring of the bound flavonolate in each complex is bent out from the plane defined by the rest of the flavonol molecule. The torsion angle of C(21)−C(22)−C(30)−C(31) is −0.914(12)° for **1**, 6.275(44)° for **3**,[14b] −9.876(7)° for **4**, and −11.030(7)° for **5**, indicating that the C(22) atom (corresponding to C(2) of the enzymatic substrate, Scheme 1) in each complex has some sp^3 character by pyramidalization, as also observed in the ES adduct of the Cu^{II}-containing 2,3-QD from *A. japonicus*.[8] The plot of the torsion angle of flavonolate vs Hammett constant σ is linear (R = 0.95) (Figure 2d), indicating that the torsion angle of flavonolate is affected by the electronic nature of the substituent group in the supporting model ligand. Such a structural and conformational change could stabilize the substrate radical formed during the reaction with O_2 and influence the electron distribution of the C(22) atom through the "electron conduit" conferred by the benzoate group, Co(II) ion, and the conjugated double bonds O(4)=C(27)−C(21)=C(22) (corresponding to O(carbonyl)=C(4)−C(3)=C(2) of the enzymatic substrate, Scheme 1; Scheme 2 in pink).

Spectroscopic and Redox Properties of the Complexes. *Infrared Spectroscopy.* In order to gain insights into the solution structure and binding mode of the carboxylate group in L^R of the complexes, FT-IR spectra of both the ethanol solution and the solid sample of the complexes were recorded (Table 3, Supporting Information Table S1 and Figure S1 for **2**). The solution spectrum of each complex is

dx.doi.org/10.1021/ic402695c | Inorg. Chem. 2014, 53, 2932−2942

Scheme 2. Products of the Reactions of Model Complexes with O_2

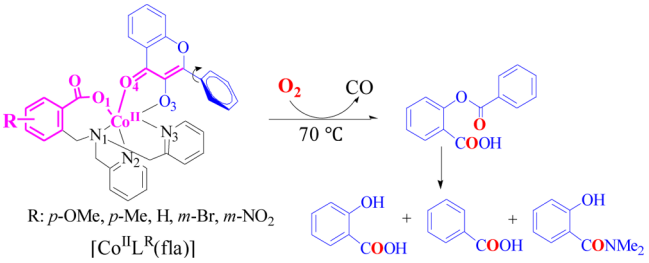

similar to that of the corresponding solid sample, and spectra of all complexes are similar to each other. Each spectrum shows a C=O stretching vibration ν(C=O) of the coordinated carbonyl group of flavonolate at ~1560 cm^{-1}, which is 40–50 cm^{-1} red shifted relative to free flavonol (1602 cm^{-1}), resembling other flavonolate complexes reported so far.[10−17] In both states, each complex shows the asymmetric $\nu_{as}(COO^-)$ and symmetric $\nu_s(COO^-)$ stretching frequencies of the carboxylate group of L^R at ~1600 and ~1410 cm^{-1}, respectively. They are also red shifted as compared with those of free ligands L^RH (~1700 and ~1600 cm^{-1}, respectively). The difference between them ($\Delta\nu = \nu_{as}(COO^-) - \nu_s(COO^-)$) is in the range of 181–200 cm^{-1}, rendering a monodentate carboxylate binding mode in all complexes in both states,[24,25] being in good agreement with the X-ray structures shown in Figure 2. It can be concluded that each complex keeps its mononuclear structure in solution, which is consistent with other spectroscopic results such as ESI-MS, EPR, and solution magnetic moment described below.

UV–vis Spectroscopy. In DMF, an intense absorption band due to the $\pi \rightarrow \pi^*$ transition of the coordinated flavonolate[26] of the complexes [$Co^{II}L^R$(fla)] appears at about 420 nm (422 nm (ε = 9.8 × 10^3 M^{-1} cm^{-1}) for **1**, 419 nm (ε = 1.1 × 10^4 M^{-1} cm^{-1}) for **2**, 415 nm (ε = 1.1 × 10^4 M^{-1} cm^{-1}) for **4**, and 413 nm (ε = 1.1 × 10^4 M^{-1} cm^{-1}) for **5** (Figure 3a and Table 3). λ_{max} values match well with those of [$Co^{II}L^H$(fla)] (**3**) (417 nm),[14b] [Co^{II}(fla)(L^1)] (L^1 = *N*-propanoate-*N*,*N*-bis(2-pyridylmethyl)amine) (423 nm),[14a] and [(6-Ph_2TPA)-Co^{II}(fla)]ClO_4 (422 nm);[13a] all are blue shifted (~40 nm) with respect to those of free flavonolate (458 nm for Me_4Nfla[13a] and 465 nm for Kfla[27]). A similar phenomenon is also observed in the enzymatic[4,6−9] and other synthetic model systems.[10−17]

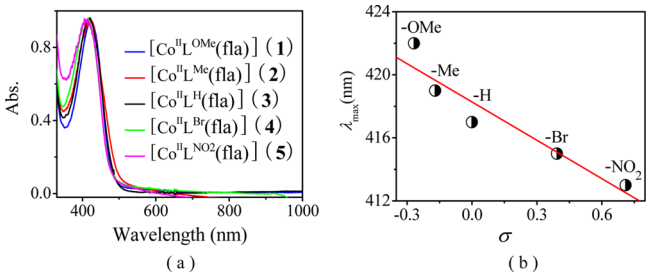

Figure 3. (a) UV–vis spectra of complexes [$Co^{II}L^R$(fla)] (~ 0.1 mM except **3** (7.2 × 10^{-2} mM) in DMF). (b) Plot of λ_{max} of the complexes vs Hammett constant σ.

Furthermore, the λ_{max} values of the complexes are in the order of [$Co^{II}L^{OMe}$(fla)] (**1**) > [$Co^{II}L^{Me}$(fla)] (**2**) > [$Co^{II}L^H$(fla)] (**3**)[14b] > [$Co^{II}L^{Br}$(fla)] (**4**) > [$Co^{II}L^{NO2}$(fla)] (**5**), and the plot of the λ_{max} vs Hammett constant σ is linear (R = 0.95) (Figure 3b). The largest λ_{max} was observed in **1**, bearing the strongest electron-donating group (OMe), presumably due to the best planarity and conjugation in flavonolate molecule of **1**, as confirmed by its smallest torsion angle. These results indicate that the λ_{max} of the coordinated flavonolate is also

Table 3. Summary of Spectroscopic and CV Data for the Complexes

		[$Co^{II}L^{OMe}$(fla)] (**1**)	[$Co^{II}L^{Me}$(fla)] (**2**)	[$Co^{II}L^{Br}$(fla)] (**4**)	[$Co^{II}L^{NO2}$(fla)] (**5**)
FT-IR					
ν(CO)/cm^{-1}		1558	1550	1560	1551
$\nu_{as}(CO_2)$/cm^{-1}		1593	1610	1610	1614
$\nu_s(CO_2)$/cm^{-1}		1412	1420	1410	1418
$\Delta\nu$/cm^{-1}		181	190	200	196
UV–vis, λ/nm (ε/M^{-1} cm^{-1})					
		277 (16 081)	277 (16 998)	277 (24 477)	269 (14 846)
		422 (9778)	419 (10 510)	415 (10 660)	413 (10 510)
		498 (71)	543 (152)	510 (182)	540 (102)
		595 (37)	605 (78)	570 (86)	630 (65)
D_q/cm^{-1}		920	879	934	845
B/cm^{-1}		939	783	835	809
ESI-MS m/z		659.1 ([$Co^{II}L^{OMe}$(fla)]H^+)	643.3 ([$Co^{II}L^{Me}$(fla)]H^+)	707.1 ([$Co^{II}L^{Br}$(fla)]H^+)	674.1 ([$Co^{II}L^{NO2}$(fla)]H^+)
		681.3 ([$Co^{II}L^{OMe}$(fla)]Na^+)	665.3 ([$Co^{II}L^{Me}$(fla)]Na^+)	729.1 ([$Co^{II}L^{Br}$(fla)]Na^+)	696.0 ([$Co^{II}L^{NO2}$(fla)]Na^+)
μ_{eff}/μ_B		4.76	4.82	5.01	4.39
CV/V					
$Co^{III/II}$	E_{pa}	−0.132	−0.123	−0.047	
	E_{pc}	−0.206	−0.181	−0.133	−0.080
	$E_{1/2}$	−0.169	−0.152	−0.090	
	i_{pc}/i_{pa}	0.88	1.06	0.79	
$fla^-/fla^\bullet$	E_{pa}	+0.315	+0.334	+0.409	+0.588
	E_{pc}	+0.225	+0.259	+0.341	+0.231
	$E_{1/2}$	+0.270	+0.297	+0.375	+0.410
	i_{pc}/i_{pa}	0.82	0.72	0.51	0.48

dx.doi.org/10.1021/ic402695c | *Inorg. Chem.* 2014, 53, 2932–2942

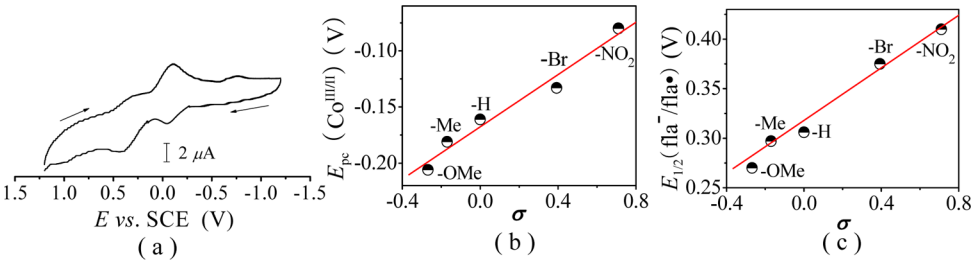

Figure 4. Cyclic voltammograms of $[Co^{II}L^{R}(fla)]$ in DMF at room temperature. (a) $[Co^{II}L^{Br}(fla)]$ (**4**) under slightly aerobic condition. (b) Plot of E_{pc} of the $Co^{III/II}$ vs Hammett constant σ. (c) Plot of $E_{1/2}$ of $fla^-/fla^\bullet$ vs Hammett constant σ.

affected by the electronic nature of the substituent group in the ligands via the "electron conduit" mentioned above.

The complexes also exhibit two weak absorption bands at about 16 950 and 20 000 cm^{-1}, respectively, which can be assigned to the spin-allowed d−d transition bands of Co^{II} ($3d^7$) in the distorted octahedral ligand field, ν_2 ($^4T_{1g}(P) \leftarrow {}^4T_{1g}(F)$) and ν_3 ($^4A_{2g} \leftarrow {}^4T_{1g}(F)$), respectively. The ligand-field constants Dq (845 − 934 cm^{-1}) and Racah parameter B (783−939 cm^{-1}) are calculated[28] (Table 3) using the observed bands ν_2 and ν_3. Both results are smaller than those of $[Co(H_2O)_6]^{2+}$ (970 cm^{-1}) and free Co^{II} ion (1030 cm^{-1}).

ESI-MS Spectroscopy. The solution structures of the complexes were also examined by ESI-MS. Each complex shows two peak clusters that can be assigned to $[Co^{II}L^{R}(^-a)]H^+$ (m/z (pos.) = 659.1 for **1**, 643.3 for **2**, 707.1 for **4**, and 674.1 for **5**) and $[Co^{II}L^{R}(fla)]Na^+$ (m/z (pos.) = 681.3 for **1**, 665.3 for **2**, 729.1 for **4**, and 696.0 for **5**); however, no carboxylate- or flavonolate-bridged dimer peak was observed. The m/z value and isotope distribution pattern of each peak cluster match well with the calculated value, indicating that each complex keeps its oxidation state and mononuclear structure in solution, which is in line with the X-ray structure and other spectroscopic results such as solution FT-IR, EPR, and solution magnetic moment results described below.

Magnetic Properties. The X-band EPR spectra of the complexes (4.0 mM in 0.5 mL DMF) were examined under N_2 at 100 K (Supporting Information Figure S2). Each complex exhibits a very weak signal at about g = 5.8 and 2.2 (Supporting Information Figure S2-A for **1**), which is akin to that of the high-spin distorted octahedral complex $[Co^{II}L^{H}(fla)]$ (**3**) (g = 5.60 and 2.25),[14b] those of the native high-spin Co^{II}-containing enzyme and its ES adduct from *Streptomyces* sp. FLA (g = 6.0, A = 95 G; g = 3.8 and 2.3),[4c] and that of the Co^{II}-containing enzyme from *B. subtilis* (g = 6.5).[4b] However, the signal of the complexes is too weak at liquid nitrogen temperature to be analyzed in detail.

^1H NMR spectra of the complexes were examined in $CDCl_3$ at ambient temperature (Supporting Information Figure S3 for **2**). In each spectrum of the complex, we observed several paramagnetically shifted weak and broad resonances over a range from −2 to 10 ppm, which are similar to those of the mononuclear complexes $[Co^{II}L^{H}(fla)]$ (**3**)[14b] and $[Co^{II}(6\text{-}Ph_2TPA)(fla)]ClO_4$.[13a]

The solution magnetic susceptibility of the complexes was also measured by NMR using Frei−Bernstein's method.[29] The solution magnetic moment of each complex was calculated to be 4.76 μ_B for **1**, 4.82 μ_B for **2**, 5.01 μ_B for **4**, and 4.39 μ_B for **5** (Table 3). The values are larger than the calculated value using the spin-only equation of the mononuclear high-spin Co^{II} center (3.87 μ_B). The difference can be explained by the contribution of the orbital moment of the Co(II) ion. The values are close to that of the nonsubstituted analogue $[Co^{II}L^{H}(fla)]\cdot CH_3OH$ (**3**) (4.13 μ_B)[14b] and also fall in the range of the reported values (4.3−5.2 μ_B) for mononuclear Co(II) complexes. These results indicate that all model complexes remain in their oxidation state and mononuclear structures in solution, which is consistent with the X-ray structure, solution FT-IR, and ESI-MS results described above.

Cyclic Voltammetry. Cyclic voltammetry of $[Co^{II}L^{R}(fla)]$ was performed in DMF at room temperature. The redox potentials (versus SCE) for all of the observed waves are listed in Table 3. For each complex there is a quasi-reversible redox couple at $E_{1/2}$ = −0.169 V (ΔE_p = 74 mV, i_{pc}/i_{pa} = 0.88) for $[Co^{II}L^{OMe}(fla)]$ (**1**), −0.152 V (ΔE_p = 58 mV, i_{pc}/i_{pa} = 1.06) for $[Co^{II}L^{Me}(fla)]$ (**2**), and −0.090 V (ΔE_p = 86 mV, i_{pc}/i_{pa} = 0.79) for $[Co^{II}L^{Br}(fla)]$ (**4**) (Figure 4a), which can be assigned to one-electron oxidation from Co^{II} to Co^{III}. The $E_{1/2}$ values are comparable with the nonsubstituted analogue $[Co^{II}L^{H}(fla)]$ (**3**) ($E_{1/2}$ = −0.062 V, ΔE_p = 201 mV, i_{pc}/i_{pa} = 0.94).[14b] For $[Co^{II}L^{NO2}(fla)]$ (**5**), we only observed a reduction wave at −0.080 V but did not observe any oxidation wave even under O_2. The E_{pc} values of $Co^{III/II}$ of the complexes show some differences in the range from −0.206 to −0.080 V (over a range of 126 mV) and are in the order of $[Co^{II}L^{OMe}(fla)]$ (**1**) < $[Co^{II}L^{Me}(fla)]$ (**2**) < $[Co^{II}L^{H}(fla)]$ (**3**) (E_{pc} = −0.162 V)[14b] < $[Co^{II}L^{Br}(fla)]$ (**4**) < $[Co^{II}L^{NO2}(fla)]$ (**5**), and the polt of E_{pc} vs Hammett constant σ is linear (R = 0.98) (Figure 4b). These results indicate that the redox potentials of the Co^{II} ion are affected by the electronic nature of the substituent group of the ligands, namely, the electron-donating group could increase the electron density around the cobalt(II) center and make it more easily oxidized.

When a DMF solution of $[Co^{II}L^{R}(fla)]$ contacted slowly with air, a new quasi-reversible redox couple appeared at $E_{1/2}$ = +0.270 V (ΔE_p = 90 mV, i_{pc}/i_{pa} = 0.82) for $[Co^{II}L^{OMe}(fla)]$ (**1**), +0.297 V (ΔE_p = 75 mV, i_{pc}/i_{pa} = 0.72) for $[Co^{II}L^{Me}(fla)]$ (**2**), +0.375 V (ΔE_p = 68 mV, i_{pc}/i_{pa} = 0.51) for $[Co^{II}L^{Br}(fla)]$ (**4**) (Figure 4a), and +0.410 V (ΔE_p = 357 mV, i_{pc}/i_{pa} = 0.48) for $[Co^{II}L^{NO2}(fla)]$ (**5**). The redox couple observed in the slow oxygenation reaction could be tentatively assigned to one-electron oxidation from fla^- to $fla^\bullet$,[14b] which are comparable with the nonsubstituted analogue $[Co^{II}L^{H}(fla)]$ (**3**) ($E_{1/2}$ = +0.306 V, ΔE_p = 180 mV, i_{pc}/i_{pa} = 0.94).[14b] The $E_{1/2}$ values of the $fla^-/fla^\bullet$ redox couples show some differences in the range from +0.270 to +0.410 V (over a range of 140 mV) and are in the order of $[Co^{II}L^{OMe}(fla)]$ (**1**) < $[Co^{II}L^{Me}(fla)]$ (**2**) < $[Co^{II}L^{H}(fla)]$ (**3**)[14b] < $[Co^{II}L^{Br}(fla)]$ (**4**) < $[Co^{II}L^{NO2}(fla)]$ (**5**), and the polt of $E_{1/2}$ of $fla^-/fla^\bullet$ vs Hammett constant σ is linear (R = 0.99) (Figure 4c). Again, the results can be explained by the electronic nature of the substituent group of the ligand. The

dx.doi.org/10.1021/ic402695c | *Inorg. Chem.* 2014, 53, 2932−2942

stronger the electron-donating group in the ligand, the more electron rich the C(22) atom (via the "electron conduit"), making the bound flavonolate more easily oxidized.

Degradation of the Complexes (Enzyme-Type Dioxygenation Reactivity). Reactions of the model complexes $[Co^{II}L^{R}(fla)]$ with O_2 in DMF at 70 °C result in two C−C bond cleavage of the *O*-heterocycle to give the ring-opening product *o*-benzoylsalicylic acid (HObs) (*m*/*z* (neg.: 241 $(M - H)^-$ and 301 $(M + OAc)^-$) (6.2−79%) (Supporting Information Figure S4) and CO[14b] as the primary products. HObs was then hydrolyzed with a small amount of water in the solvent and amidated by the solvent DMF to give salicylic acid (*m*/*z* (neg.) 137 $(M - H)^-$) (13 − 76%), benzoic acid (*m*/*z* (neg.) 121 $(M - H)^-$) (19−89%) and 2-hydroxy-*N*,*N*-dimethylbenzamide (*m*/*z* (pos.) 166 $(M + H)^+$) (8.3−48%) as the final products (Scheme 2, characterized by HPLC-MS and HPLC, results seen in Supporting Information Table S2). Conversions of the complexes are over 95%.

The dioxygenation reaction of the complexes was followed by monitoring the decrease of the absorbance of the coordinated flavonolate ($\pi \rightarrow \pi^*$ transition) at the corresponding λ_{max} (Figure 5a for **1**, Figure 3a, Table 3). Experimental conditions and the observed initial rates are summarized in Supporting Information Table S3. The initial reaction rate of each complex exhibits a linear relationship with respect to the initial concentrations of both $[Co^{II}L^{R}(fla)]$ (Figure 5b) and O_2 (Figure 5c), so the rate law could be determined as $-d[Co^{II}L^{R}(fla)]/dt = k[Co^{II}L^{R}(fla)][O_2]$. The second-order reaction rate constants *k* were thus determined as 9.60−49.4 × 10^{-2} M^{-1} s^{-1} at 70 °C ($\Delta H^{\ddagger}$ = 72−86 kJ mol^{-1}, $\Delta S^{\ddagger}$ = −15 to −43 J mol^{-1} K^{-1}) (Table 4, Supporting Information Table S3 and Figure S5). To date, two examples of Co(II)−flavonolate complexes bearing dioxygenation reactivity, $[Co^{II}(fla)(L^{1})]$ (2.09 × 10^{-2} M^{-1} s^{-1} at 80 °C, not structurally characterized)[14a] and $[Co^{II}L^{H}(fla)]$ (**3**) (34.0 × 10^{-2} M^{-1} s^{-1} at 70 °C),[14b] were reported. Other reported ES model complexes exhibit lower reactivity and require higher temperature (65−130 °C).[10−16,17b,c] Compared with them, our model complexes show higher reactivity at lower temperature (55−85 °C), which can be attributed to the existing carboxylate group in the ligand.

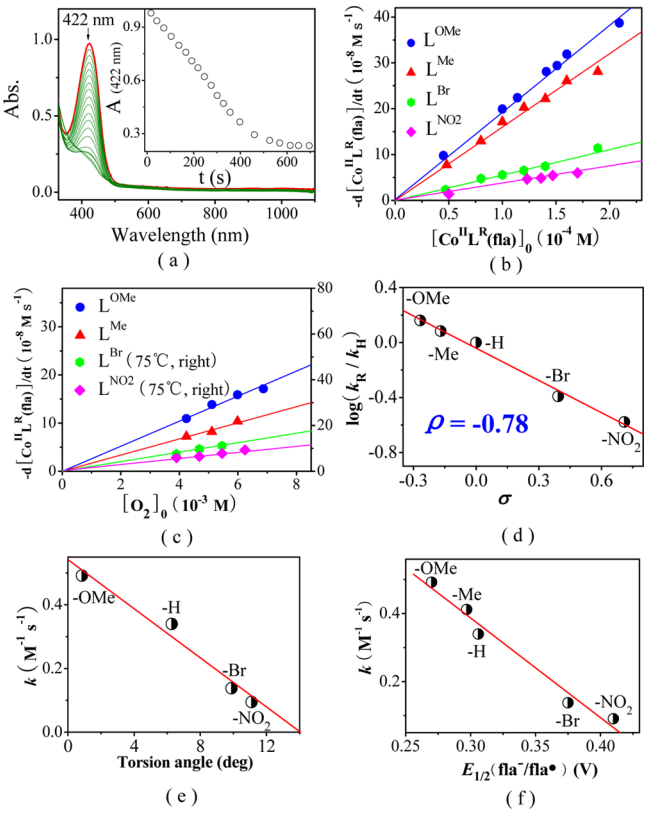

Figure 5. Dioxygenation of the $[Co^{II}L^{R}(fla)]$ complexes at 70 °C under O_2. (a) Spectral change observed upon introduction of O_2 gas into a DMF solution of $[Co^{II}L^{OMe}(fla)]$ (**1**) (1.0 × 10^{-4} M). (Inset) Time course of the absorption changes of $[Co^{II}L^{OMe}(fla)]$ (**1**) at 422 nm. (b) Plot of $-d[Co^{II}L^{R}(fla)]/dt$ vs $[Co^{II}L^{R}(fla)]_0$. (c) Plot of $-d[Co^{II}L^{R}(fla)]/dt$ vs $[O_2]_0$. (d) Hammett plot of the dioxygenation of $[Co^{II}L^{R}(fla)]$. (e) Plot of *k* vs torsion angle of flavonolate. (f) Plot of *k* vs $E_{1/2}$ of fla^-/$fla^{\bullet}$.

In order to get insights into the carboxylate effects of the model ligand, the noncarboxylate group analogue $[Co^{II}L_0(fla)(CH_3O)]$ (L_0 = benzyl-bis-pyridin-2-ylmethyl-amine) supported by the 3N chelating ligand was synthesized and characterized (Supporting Information). The band of the $\pi \rightarrow \pi^*$ transition of the coordinated flavonolate appears at 416 nm (ε = 11 614 M^{-1} cm^{-1}) (Supporting Information Figure S5a), which is a little blue shifted compared with that of the *o*-carboxylate group substituted analogue $[Co^{II}L^{H}(fla)]$ (**3**)[14b] (417 nm). The reactivity of $[Co^{II}L_0(fla)(CH_3O)]$ toward dioxygen was also examined (Supporting Information Table S3). The plots of the initial reaction rate vs the initial concentrations of both $[Co^{II}L_0(fla)(CH_3O)]$ and O_2 are linear (Supporting Information Figure S5b and S5c). Thus, the rate law also can be described as $-d[Co^{II}L_0(fla)(CH_3O)]/dt = k[Co^{II}L_0(fla)(CH_3O)][O_2]$. The second-order reaction rate constant *k* is 7.20 × 10^{-2} M^{-1} s^{-1} at 70 °C ($\Delta H^{\ddagger}$ = 90.14 kJ mol^{-1}, $\Delta S^{\ddagger}$ = −5.12 J mol^{-1} K^{-1}) (Table 4 and Supporting Information Figure S6), much smaller (about 5 times) than that of the *o*-carboxylate group substituted analogue $[Co^{II}L^{H}(fla)]$ (**3**).[14b] These results clearly indicate that the presence of carboxylate group in the ligand can enhance the reactivity via lowering the redox potential of the coordinated flavonolate by electron donation.

Although the structures of the ES model complexes $[Co^{II}L^{R}(fla)]$ are similar, the dioxygenation reactivity of $[Co^{II}L^{R}(fla)]$ shows some differences and is in the order of $[Co^{II}L^{OMe}(fla)]$ (**1**) > $[Co^{II}L^{Me}(fla)]$ (**2**) > $[Co^{II}L^{H}(fla)]$ (**3**)[14b] > $[Co^{II}L^{Br}(fla)]$ (**4**) > $[Co^{II}L^{NO2}(fla)]$ (**5**) (Figure 5), and the Hammett plot is linear (ρ = −0.78) (Figure 5d). This order is reverse of the order of the torsion angle of flavonolate and the $E_{1/2}$ of fla^-/$fla^{\bullet}$ described above, and the plot of *k* vs each of them (Figure 5e (*R* = 0.99) and 5f (*R* = 0.99), respectively) is linear. All these correlations provide evidence that the structure, property, and dioxygenation reactivity of the model complexes were influenced by the electronic nature of the substituent group in the ligand via the "electron conduit", and there is some relationship among them, providing important insights into the structure−property−reactivity relationship.

In fact, when the CH_2Cl_2/MeOH solutions of $[Co^{II}L^{R}(fla)]$ were exposed to air at room temperature, we initially observed a $[Co^{III}L^{R}(fla)]^+$ peak cluster in ESI-MS spectra (Table 5) and the $\pi \rightarrow \pi^*$ transition band of flavonolate (∼ 0.1 mM) disappeared after 1 day, indicating that our model complexes are also active in CH_2Cl_2/MeOH. Such phenomenon inspires us to check the solvent effects on the dioxygenation reactivity of the complexes. Thus, the same dioxygenation reaction of $[Co^{II}L^{OMe}(fla)]$ but in CH_2Cl_2/MeOH (0.1 mM in 50 mL of

dx.doi.org/10.1021/ic402695c | Inorg. Chem. 2014, 53, 2932−2942

Table 4. Kinetic Data (at 70 °C) and Activation Parameters of the Complexes

complexes	10^2k (M^{-1} s^{-1})	$\Delta H^{\ddagger}$ (kJ mol^{-1})	$\Delta S^{\ddagger}$ (J mol^{-1} K^{-1})	E_a (kJ mol^{-1})
$[Co^{II}L^{OMe}(fla)]$ (**1**)	49.4 ± 0.24	71.96	−41.87	74.75
$[Co^{II}L^{Me}(fla)]$ (**2**)	40.5 ± 0.17	72.77	−42.69	75.58
$[Co^{II}L^{Br}(fla)]$ (**4**)	13.7 ± 0.10	84.69	−16.19	87.53
$[Co^{II}L^{NO2}(fla)]$ (**5**)	9.60 ± 0.04	85.93	−15.02	88.85
$[Co^{II}L_0(fla)]$	7.20 ± 0.03	90.14	−5.120	93.08

Table 5. ESI-MS Results of the Complexes When Exposed to Air and after Reaction with O_2

		$[Co^{II}L^{OMe}(fla)]$ (**1**)	$[Co^{II}L^{Me}(fla)]$ (**2**)	$[Co^{II}L^{Br}(fla)]$ (**4**)	$[Co^{II}L^{NO2}(fla)]$ (**5**)
ESI-MS (m/z (pos.))	exposed to air	658.3 ($[Co^{III}L^{OMe}(fla)]^+$)	642.3 ($[Co^{III}L^{Me}(fla)]^+$)	706.1 ($[Co^{III}L^{Br}(fla)]^+$)	673.1 ($[Co^{III}L^{NO2}(fla)]^+$)
	after reaction	542.2 $[Co^{III}L^{OMe}(ben)]^+$	542.2 $[Co^{III}L^{Me}(sal)]^+$	590.0 $[Co^{III}L^{Br}(ben)]^+$	573.1 $[Co^{III}L^{NO2}(sal)]^+$

1:1 CH_2Cl_2/MeOH, reflux for 14 h) and DMSO (1 mM in 10 mL of DMSO, at 130 °C for 48 h) was performed, and their products were characterized by HPLC-MS and HPLC. In both reactions the same enzyme-type dioxygenation ring-opening products as that in DMF were observed (HObs (m/z (neg.) 241 $(M - H)^-$) (29.6% and 28.5%), salicylic acid (m/z (neg.) 137 $(M - H)^-$) (32.6% and 18.5%), benzoic acid (m/z (neg.) 121 $(M - H)^-$) (34.1% and 17.4%), shown in Scheme 2, Supporting Information Table S2 and Figure S7). Besides, some unoxidized substrate flavonol (m/z (neg.) 237 $(M)^-$; 33.1% and 48.5%, respectively) was also detected, and the total conversions were 64% and 47%, respectively. The kinetic result shows that the dioxygenation reaction of $[Co^{II}L^{OMe}(fla)]$ in DMSO is much slower (k about 3.0×10^{-2} M^{-1} s^{-1} at 100 °C, Supporting Information Figure S8) than that in DMF (k 49.4×10^{-2} M^{-1} s^{-1} at 70 °C). These results clearly indicate that the same but much slower dioxygenation reaction occurs both in CH_2Cl_2/MeOH and in DMSO. Thus, CH_2Cl_2/MeOH and DMSO are not suitable solvents for the kinetic study.

Dioxygenation Reaction Mechanism. Compared with the free ion, the Co^{II} ion in the Co^{II}–flavonolate complex is more easily oxidized to Co^{III}, which can be explained by the electron donation contribution of the coordinated flavonolate and ligand. In fact, when the $[Co^{II}L^{R}(fla)]$ solution was exposed to air, we initially observed a peak cluster $[Co^{III}L^{R}(fla)]^+$ (Table 5), indicating that the Co^{II} ion was oxidized by O_2 to Co^{III} to form the Co^{III}–flavonolate species $[Co^{III}L^{R}(fla)]^+$ (**A**) at the first stage of the reaction, and the O_2 was reduced to $O_2^{\bullet-}$ (superoxide radical), as proved by the reaction with nitroblue tetrazolium (NBT^{2+}). Significantly, when excess NBT^{2+} was added to the O_2-saturated $[Co^{II}L^{R}(fla)]$ solution, a new absorption band arose at 530 nm (Figure 6, blue line for **1**). It can be assigned to the monoformazan (MF^+) due to reduction of NBT^{2+} by free $O_2^{\bullet-}$ generated in the reaction of $[Co^{II}L^{R}(fla)]$ with O_2.[30]

Then $[Co^{III}L^{R}(fla)]^+$ (**A**) is proposed to react with another O_2 molecule to form a radical species $[Co^{III}L^{R}(fla^{\bullet})]^+$ (**B**) and another $O_2^{\bullet-}$ (Scheme 3, step 2). In order to prove this postulation, we synthesized the Co^{III}–flavonolate analogue $[Co^{III}L^{OMe}(fla)](OAc)$ independently, checked its reaction with dioxygen (2.0×10^{-3} M in 2 mL of DMF, at 70 °C for 8h), and observed $O_2^{\bullet-}$ by NBT^{2+} (Figure 6 red line) as well as the same enzyme-type ring-opening products (salicylic acid 31.5%, benzoic acid 16.1%, *N*,*N*-dimethylbenzamide 21.0%, and HObs 62.3%, conversion 94%). Thus, step 2 in Scheme 3 was proved.

After the dioxygenation reaction of $[Co^{II}L^{R}(fla)]$, we observed a peak cluster of $[Co^{III}L^{R}(prod)]^+$ (prod = ben

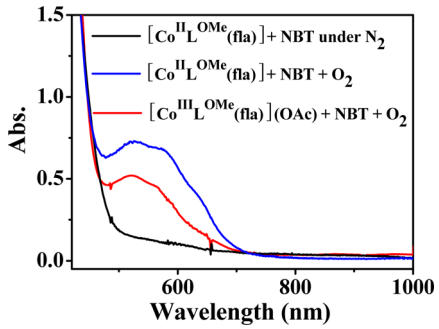

Figure 6. Spectral change of $[Co^{II}L^{OMe}(fla)]$ and $[Co^{III}L^{OMe}(^{-}a)]$-(OAc) (1.0 mM in DMF) in the presence of excess NBT under O_2 (blue and red) and N_2 (black) at room temperature.

(benzoate) or sal (salicylate), one of the oxidation products, Table 5) and the weak Co^{II} EPR signal disappeared (Supporting Information Figure S2-B). These results indicate that a fast radical–radical reaction exists between the generated $[Co^{III}L^{R}(fla^{\bullet})]^+$ (B) and $O_2^{\bullet-}$, which leads to the dioxygenated enzyme-type ring-opening free organic products (Scheme 2) and coordinated products complex $[Co^{III}L^{R}(prod)]^+$ with concomitant release of CO.

On the basis of the structure, spectroscopic, redox properties, kinetic, and products analysis results, we proposed the dioxygenation mechanism (Scheme 3) as follows. First, $[Co^{II}L^{R}(fla)]$ may react with one O_2 molecule to produce $[Co^{III}L^{R}(fla)]^+$ (A) and $O_2^{\bullet-}$ quickly. The following step is a rate-determining one-electron transfer from the bound fla^- to another O_2 molecule to form $[Co^{III}L^{R}(fla^{\bullet})]^+$ (B) and another $O_2^{\bullet-}$. The final step is a fast radical–radical reaction, forming the dioxygenated products and releasing CO. The mechanisms of the complexes are similar each other and also similar to that of the nonsubstituted analogue $[Co^{II}L^{H}(fla)]$ (**3**).[14b]

Although the oxidation state change of the metal center Co^{II} ion is not observed by EPR in the native Co-2,3-QD, there still exists the possibility that one-electron transfer from the substrate flavonol via the Co^{II} ion to dioxygen is triggered by dioxygen binding with a "transient change of the oxidation state of the metal center".[4c] Unfortunately, such an oxidation state change could not be detected by the conventional experimental method. In comparison, our mechanism is similar to that of Co–2,3-QD except the oxidation state change in the first step.

CONCLUSIONS

In summary, we designed and synthesized a series of Co^{II}–flavonolate complexes $[Co^{II}L^{R}(fla)]$ (R = *p*-OMe (**1**), *p*-Me (**2**), *m*-Br (**4**), and *m*-NO_2 (**5**)) as structural and functional ES

dx.doi.org/10.1021/ic402695c | Inorg. Chem. 2014, 53, 2932–2942

Scheme 3. Proposed Dioxygenation Reaction Mechanism of Model Complexes $[Co^{II}L^{R}(fla)]$

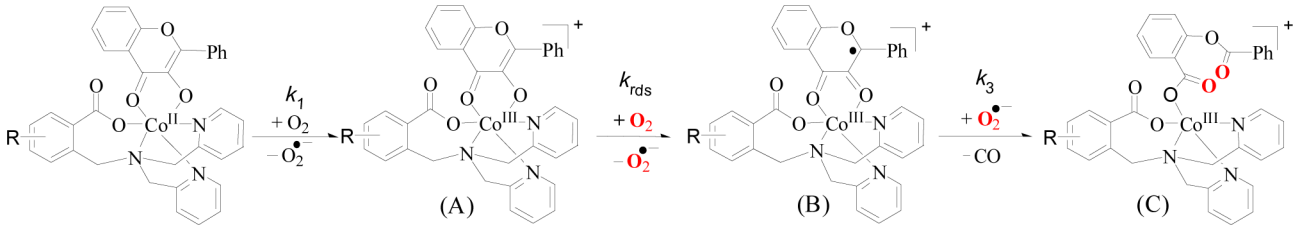

models for the active site of Co−2,3-QD. Their structures, spectroscopic futures, redox properties, and reactivity toward dioxygen were investigated in detail. The reaction of each model complex with O_2 shows high enzyme-type dioxygenation reactivity (oxidative *O*-heterocyclic ring opening of the bound substrate flavonolate) at low temperature and first-order dependence versus the initial concentrations of both complex and O_2. The reactivity is remarkably promoted by the carboxylate group in the supporting model ligand by electron donation. Besides, it also exhibits a substituent group dependent order of −OMe (**1**) > −Me (**2**) > −H (**3**)[14b] > −Br (**4**) > $-NO_2$ (**5**), and the Hammett plot is linear (ρ = −0.78). The structures, properties, and reactivity of the model complexes are all influenced by the electronic nature of the substituent group in the ligand via the benzoate, Co(II) ion, and O(4)═C(27)−C(21)═C(22) "electron conduit". A stronger electron-donating group in the ligand may induce a smaller torsion angle between the B and the C ring, larger λ_{max} of the $\pi \rightarrow \pi^*$ transition, lower redox potential of flavonolate, and finally higher reactivity of the model complexes. As the first example of a series of structural and functional ES models of Co-2,3-QD, our study focuses on both the electronic substituent and the carboxylate effects of the supporting model ligands on the enzyme-type dioxygenation reactivity and will provide important insights into the structure−property−reactivity relationship, the electronic and carboxylate effects on the enzymatic reactivity, the role of metal ion, and the catalytic role of Co−2,3-QD.

■ ASSOCIATED CONTENT

Ⓢ Supporting Information

Ligands synthesis, reaction products analysis data, kinetic data, FT-IR, EPR, ^{1}H NMR, LC-MS spectra, Eyring plot, and crystallographic information (CIF) CCDC 957283 for **1**, 957282 for **4**, and CCDC 957281 for **5**. This material is available free of charge via the Internet at http://pubs.acs.org.

■ AUTHOR INFORMATION

Corresponding Author

*E-mail: yingjis@dlut.edu.cn.

Notes

The authors declare no competing financial interest.

■ ACKNOWLEDGMENTS

We gratefully acknowledge the financial support of the National Natural Science Foundation of China (Nos. 20641002, 20771020, 20811140328) and the Fundamental Research Funds for the Central Universities (DUT12YQ04).

■ REFERENCES

(1) Roth, J. R.; Lawrence, J. G.; Bobik, T. A. *Annu. Rev. Microbiol.* **1996**, *50*, 137−181.

(2) (a) Moratal, J. M.; Martínez-Ferrer, M. J.; Donaire, A.; Aznar, L. *J. Inorg. Biochem.* **1992**, *45*, 65−71. (b) Ciancaglini, P.; Pizauro, J. M.; Leone, F. A. *J. Inorg. Biochem.* **1995**, *60*, 155−162. (c) Ben-Meir, D.; Spungin, A.; Ashkenazi, R.; Blumberg, S. *Eur. J. Biochem. FEBS* **1993**, *212*, 107−112. (d) Luchinat, C.; Monnanni, R.; Roelens, S.; Vallee, B. L.; Auld, D. S. *J. Inorg. Biochem.* **1988**, *32*, 1−6.

(3) (a) Mills, S. A.; Klinman, J. P. *J. Am. Chem. Soc.* **2000**, *122*, 9897−9904. (b) Fielding, A. J.; Kovaleva, E. G.; Farquhar, E. R.; Lipscomb, J. D.; Que, L., Jr. *J. Biol. Inorg. Chem.* **2011**, *16*, 341−355. (c) Dai, Y.; Wensink, P. C.; Abeles, R. H. *J. Biol. Chem.* **1999**, *274*, 1193−1195.

(4) (a) Gopal, B.; Madan, L. L.; Betz, S. F.; Kossiakoff, A. A. *Biochemistry* **2005**, *44*, 193−201. (b) Schaab, M. R.; Barney, B. M.; Francisco, W. A. *Biochemistry* **2006**, *45*, 1009−1016. (c) Merkens, H.; Kappl, R.; Jakob, R. P.; Schmid, F. X.; Fetzner, S. *Biochemistry* **2008**, *47*, 12185−12196.

(5) Wollenweber, E. *Flavonoids: Advances in Research*; Harborne, J. B., Mabry, T. J., Eds.; Chapman & Hall: London, U.K., 1982.

(6) Fusetti, F.; Schröter, K. H.; Steiner, R. A.; van Noort, P. I.; Pijning, T.; Rozeboom, H. J.; Kalk, K. H.; Egmond, M. R.; Dijkstra, B. W. *Structure* **2002**, *10*, 259−268.

(7) (a) Laura, B.; Shirley, A. F.; Victoria, J. J.; Stephen, B. *FEBS Lett.* **2004**, *557*, 45−48. (b) Barney, B. M.; Schaab, M. R.; LoBrutto, R.; Francisco, W. A. *Protein Expr. Purif.* **2004**, *35*, 131−141.

(8) Steiner, R. A.; Kalk, K. H.; Dijkstra, B. W. *Proc. Natl. Acad. Sci.* **2002**, *99*, 16625−16630.

(9) (a) Steiner, R. A.; Kooter, I. M.; Dijkstra, B. W. *Biochemistry* **2002**, *41*, 7955−7962. (b) Antonczak, S.; Fiorucci, S.; Golebiowski, J.; Cabrol-Bass, D. *Phys. Chem. Chem. Phys.* **2009**, *11*, 1491−1501.

(10) (a) Kaizer, J.; Balogh-Hergovich, E.; Czaun, M.; Casy, T.; Speier, G. *Coord. Chem. Rev.* **2006**, *222*, 2222−2233. (b) Pap, J. S.; Kaizer, J.; Speier, G. *Coord. Chem. Rev.* **2010**, *254*, 781−793. (c) Kaizer, J.; Pap, J. S; Speier, G. Copper Dioxygenases. In *Copper-Oxygen Chemistry*; Karlin, K. D., Shinobu, I., Eds.; John Wiley & Sons, Inc.: Hoboken, NJ, 2011; pp 23−52. (d) Balogh-Hergovich, É.; Kaizer, J.; Speier, G.; Argay, G.; Párkányi, L. *J. Chem. Soc., Dalton Trans.* **1999**, 3847−3854. (e) Balogh-Hergovich, É.; Kaizer, J.; Pap, J.; Speier, G.; Huttner, G.; Zsolnai, L. *Eur. J. Inorg. Chem.* **2002**, 2287−2295. (f) Balogh-Hergovich, É.; Kaizer, J.; Speier, G.; Fülöp, V.; Párkányi, L. *Inorg. Chem.* **1999**, *38*, 3787−3795.

(11) (a) Kaizer, J.; Barath, G.; Pap, J. S.; Speier, G. *Chem. Commun.* **2007**, 5235−5237. (b) Kaizer, J.; Pap, J. S.; Speier, G. *On Biomimetics*; Pramatarova, L. D., Ed.; Intech Open Access Publisher: New York, 2011; pp 29−42. (c) Baráth, G.; Kaizer, J.; Speier, G.; Párkányi, L.; Kuzmann, E.; Vértes, A. *Chem. Commun.* **2009**, 3630−3632.

(12) (a) Nishinaga, A.; Tojo, T.; Matsuura, T. *J. Chem. Soc., Chem. Commun.* **1974**, 896−897. (b) Nishinaga, A.; Numada, N.; Maruyama, K. *Tetrahedron Lett.* **1989**, *30*, 2257−2258. (c) Hiller, W.; Nishinaga, A.; Rieker, A. *Z. Naturforsch., B: Chem. Sci.* **1992**, *47*, 1185−1188. (d) Nishinaga, A.; Kuwashige, T.; Tsutsui, T.; Mashino, T.; Maruyama, K. *J. Chem. Soc., Dalton Trans.* **1994**, 805−810.

(13) (a) Grubel, K.; Rudzka, K.; Arif, A. M.; Klotz, K. L.; Halfen, J. A.; Berreau, L. M. *Inorg. Chem.* **2010**, *49*, 82−96. (b) Grubel, K.; Marts, A.; Greer, S. M.; Tierney, D. L.; Allpress, C. J.; Anderson, S. N.; Laughlin, B. J.; Smith, R. C.; Arif, A. M.; Berreau, L. M. *Eur. J. Inorg. Chem.* **2012**, 4750−4757. (c) Grubel, K.; Laughlin, B. J.; Maltais, T. R.; Smith, R. C.; Arif, A. M.; Berreau, L. M. *Chem. Commun.* **2011**, *47*, 10431−10433.

(14) (a) Matuz, A.; Giorgi, M.; Speier, G.; Kaizer, J. *Polyhedron* **2013**, *63*, 41−49. (b) Sun, Y.-J.; Huang, Q.-Q.; Tano, T.; Itoh, S. *Inorg. Chem.* **2013**, *52*, 10936−10948.
(15) Barhacs, L.; Kaizer, J.; Speier, G. *J. Mol. Catal. A.* **2001**, *172*, 117−125.
(16) Balogh-Hergovich, É.; Kaizer, J.; Speier, G. *J. Mol. Catal. A.* **2003**, *206*, 83−87.
(17) (a) Aramice, Y. S.; Malkhasian, F. M. E.; Nikolovski, B.; Menon, A.; Kucera, B. E.; Chavez, F. A. *Inorg. Chem.* **2007**, *46*, 2950−2952. (b) Kaizer, J.; Góger, S.; Speier, G.; Réglier, M.; Giorgi, M. *Inorg. Chem. Commun.* **2006**, *9*, 251−254. (c) Volkman, J.; Nicholas, K. M. *Tetrahedron* **2012**, *68*, 3368−3376.
(18) Armarego, W. L. F.; Perrin, D. D. *Purification of Laboratory Chemicals*, 4th ed.; Butterworth-Heinemann: Oxford, U.K., 1996.
(19) (a) *Program for the Solution of Crystal Structures*; University of Gottingen: Gottingen, Germany, 1997. (b) *Program for the Refinement of Crystal Structures*; University of Gottingen: Gottingen, Germany, 1997.
(20) Kruis, A. *Landolt-Börnstein*; Springer-Verlag: Berlin, 1976; Board 4, Teil 4, p 269.
(21) Ram, G.; Sharaf, A. R. *J. Ind. Chem. Soc.* **1968**, *45*, 13−16.
(22) Brydon, P. *Philos. Mag. Lett.* **1999**, *79*, 383−387.
(23) Etter, M. C.; Urbanczyk-Lipkowska, Z.; Baer, S.; Barbara, P. F. *J. Mol. Struct.* **1986**, *144*, 155−167.
(24) Christou, G.; Perlepes, S. P.; Libby, E.; Folting, K.; Huffman, J. C.; Webb, R. J.; Hendrickson, D. N. *Inorg. Chem.* **1990**, *29*, 3657−3666.
(25) Chadjistamatis, I.; Terzis, A.; Raptopoulou, C. P.; Perlepes, S. P. *Inorg. Chem. Commun.* **2003**, *6*, 1365−1371.
(26) Jurd, L.; Geissman, T. A. *J. Org. Chem.* **1956**, *21*, 1395−1401.
(27) (a) Barhács, L.; Kaizer, J.; Speier, G. *J. Org. Chem.* **2000**, *65*, 3449−3452. (b) Pap, J. S.; Matuz, A.; Baráth, G.; Kripli, B.; Giorgi, M.; Speier, G.; Kaizer, J. *J. Inorg. Biochem.* **2012**, *108*, 15−21.
(28) Lever, A. B. P. *Inorgnic Electronic Spectroscopy*, 2nd ed.; Elsevier: Amsterdam, 1984.
(29) (a) Freit, K.; Bernstein, H. J. *J. Chem. Phys.* **1962**, *37*, 1891−1892. (b) Kuchel, P. W.; Chapman, B. E.; Bubb, W. A.; Hansen, P. E.; Dur, C. J. *Concepts Magn. Reson.* **2003**, *A 18*, 56−71.
(30) Blelski, B. H. J.; Shiue, G. G.; Bajuk, S. *J. Phys. Chem.* **1980**, *84*, 830−833.

dx.doi.org/10.1021/ic402695c | *Inorg. Chem.* 2014, 53, 2932−2942